Supplementary Information

Interplay between the Westerlies and Asian monsoon recorded in Lake Qinghai sediments since 32 ka

An Zhisheng[1 2*], Steven M. Colman[3], Weijian Zhou[1], Xiaoqiang Li[1], Eric T. Brown[3], A. J. Timothy Jull[4], Yanjun Cai[1], Yongsong Huang[5], Xuefeng Lu[1], Hong Chang[1], Yougui Song[1], Youbin Sun[1], Hai Xu[1], Weiguo Liu[1], Zhangdong Jin[1], Xiaodong Liu[1], Peng Cheng[1], Yu Liu[1], Li Ai[1], Xiangzhong Li[1], Xiuju Liu[3], Libin Yan[1], Zhengguo Shi[1], Xulong Wang[1], Feng Wu[1], Xiaoke Qiang[1], Jibao Dong[1], Fengyan Lu[1], Xinwen Xu[1]

[1] State Key Laboratory of Loess and Quaternary Geology, Institute of Earth Environment, Chinese Academy of Sciences, Xi'an, 710075, China;

[2] Department of Environmental Science & Engineering, Fudan University, Shanghai 200433, China

[3] Large Lakes Observatory and Department of Geological Sciences, University of Minnesota Duluth, Duluth, MN 55812, USA;

[4] NSF Arizona AMS Facility, University of Arizona, Tucson, AZ 85721, USA;

[5] Department of Geological Sciences, Brown University, Providence, Rhode Island 02912, USA

*Corresponding author: anzs@loess.llqg.ac.cn

Supplementary Figures

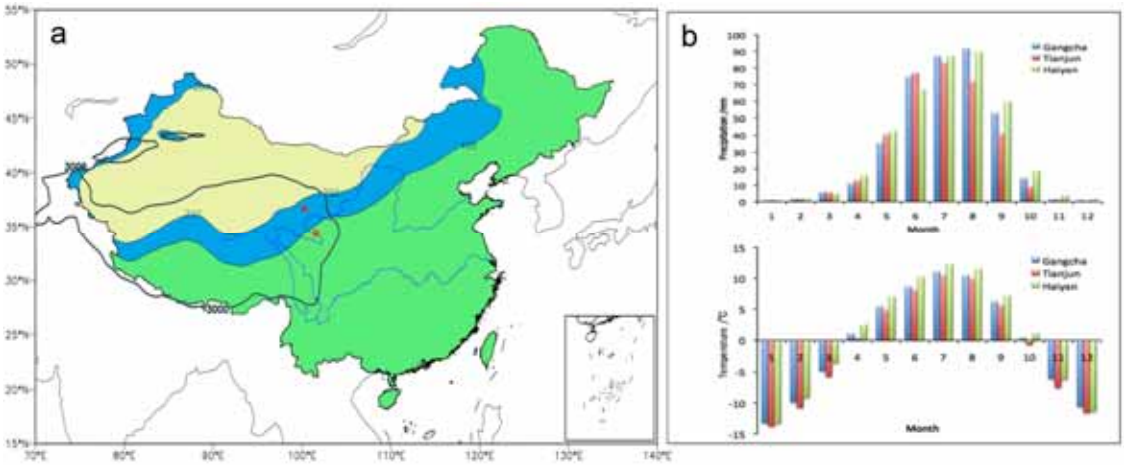

Fig. S1 a) Distribution of modern monsoonal and arid/semi-arid areas in China. The blue shaded area denotes the transitional/semi-arid zone between humid (green, controlled by the Asian monsoon) and arid inland areas (yellow, influenced by the Westerlies) in China, where the mean annual precipitation is 200-400 mm (S1). The black contour shows the extent of the Tibetan Plateau above the elevation of 3000 m. The red triangle and red circle show the locations of Lake Qinghai, and Xiannv cave (34°27'N, 101°26'E, elevation 3730 m, ~250 km southeast of Lake Qinghai), respectively. **b)** Mean monthly precipitation and temperature averaged for 1976-2007 from three meteorological stations within the Lake Qinghai catchment (Gangcha, 37°19'N, 100°10'E; Tianjun, 37°17'N, 99°2'E; Haiyan, 36°53'N, 100°59'E). Mean annual precipitation is dominated by precipitation in June, July and August, which make up about 65% of the total of 373 mm, showing the clear seasonality of monsoonal precipitation. The mean annual temperature of three stations is ~ -0.1℃.

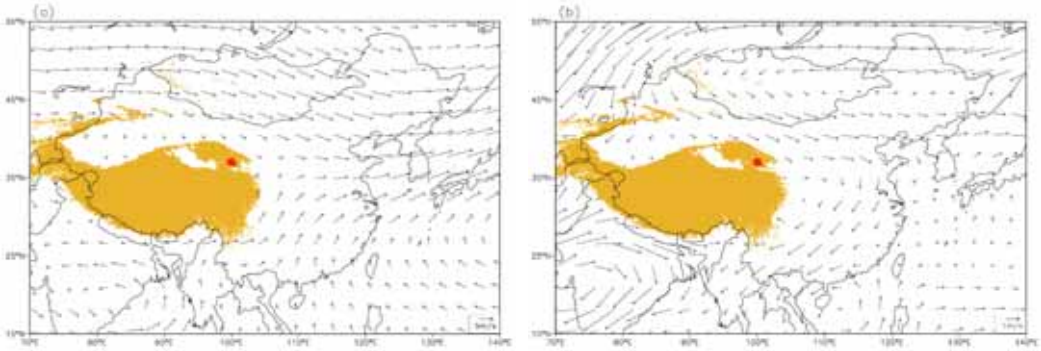

Fig. S2 a) 700 hPa wind fields in summer (JJA) during the pre-industrial (PI) period based on the CCSM3 modeling output in the framework of PMIP2 (S2). The results show that the summer monsoon reached Lake Qinghai in PI summer; **b**) Difference of CCSM3-simulated 700 hPa wind fields between LGM and PI summers, showing a weakened Asian summer monsoon and a strengthened Westerly wind around Lake Qinghai in LGM summer compared with the PI summer. Red solid circles represent the location of Lake Qinghai. The elevations of yellow areas exceed 3000 m.

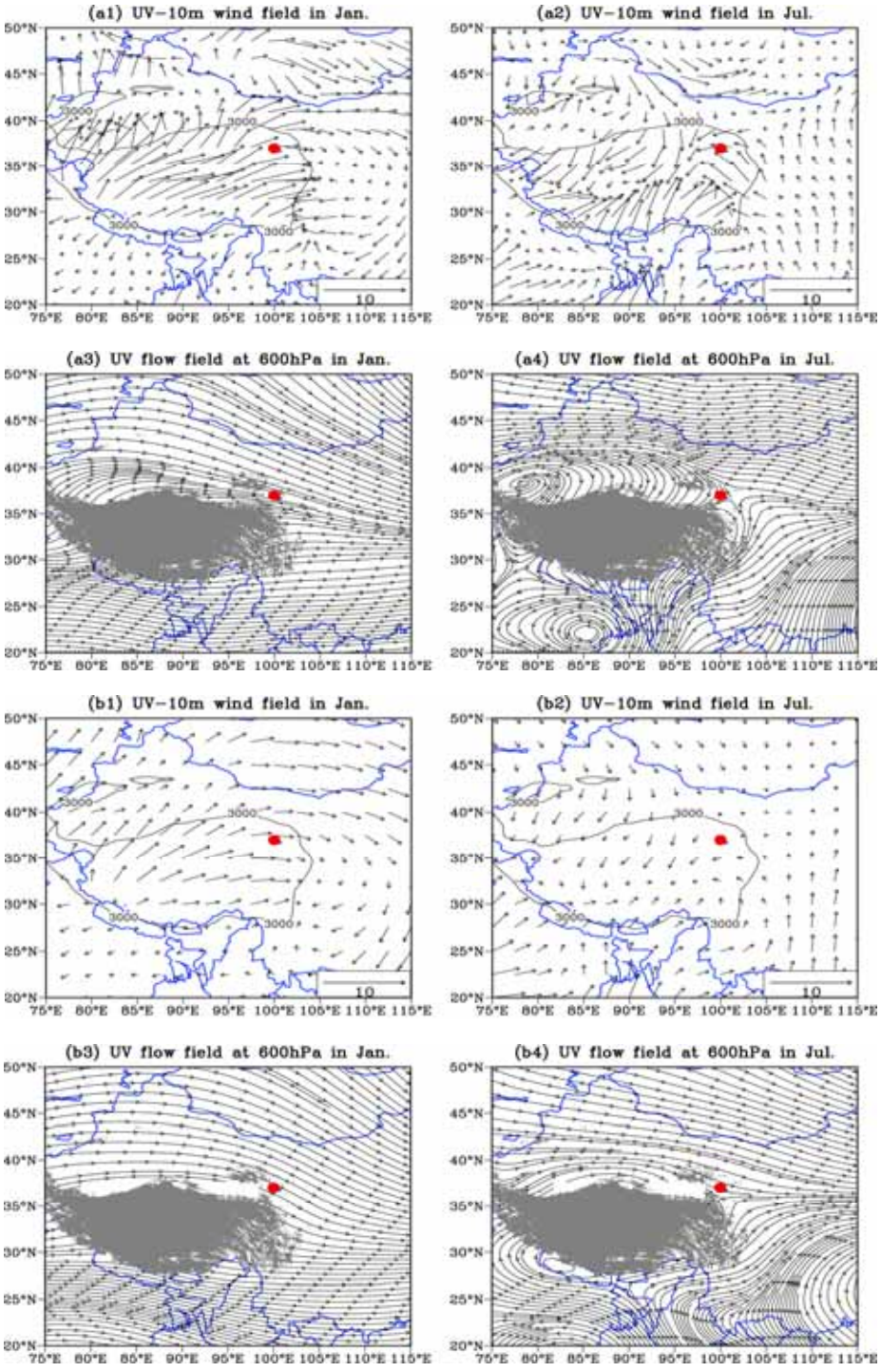
(a1) UV−10m wind field in Jan.
(a2) UV−10m wind field in Jul.
(a3) UV flow field at 600hPa in Jan.
(a4) UV flow field at 600hPa in Jul.
(b1) UV−10m wind field in Jan.
(b2) UV−10m wind field in Jul.
(b3) UV flow field at 600hPa in Jan.
(b4) UV flow field at 600hPa in Jul.
50°N
45°N
40°N
35°N
30°N
25°N
20°N
75°E 80°E 85°E 90°E 95°E 100°E 105°E 110°E 115°E
3000
10

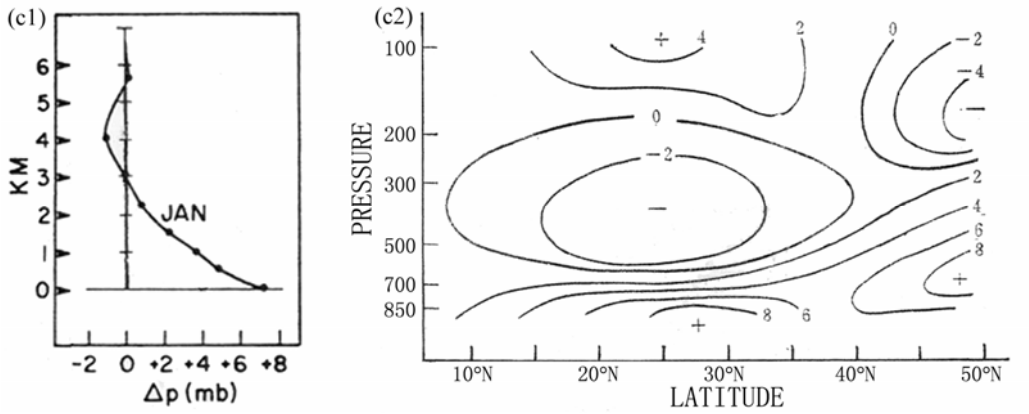

Fig. S3 Averaged surface 10-meter wind fields (a1, a2) and flow fields at 600 hPa (a3, a4) in Jan. (a1, a3) and in Jul. (a2, a4) from 1971 to 2000 (S3). Averaged surface 10-meter wind fields (b1, b2) and flow fields at 600 hPa (b3, b4) in Jan. (b1, b3) and in Jul. (b2, b4) during the LGM from PMIP2 (S2). Red solid circle indicates the location of Lake Qinghai (36°32'-37°15'N, 99°36'-100°47'E, elevation 3194 m). The black contour in (a1-2, b1-2) denotes elevation of 3000 meters. The grey shaded area in (a3-4, b3-4) indicates the region where the elevation exceeds 4000 meters. (c1): Vertical profile of summed-up pressure differentials (ΔP*) across the Tibetan Plateau (positive corresponds to eastward pressure torque on the atmosphere). Modified after Fig.1 by Newton (1971) (S4). (c2): Temperature difference between the eastern and western sides of the Tibetan Plateau in March ($T_{60°E}$-$T_{120°E}$). Units of °C, ordinate in log-pressure, abscissa in latitude. Modified after Fig. 13.10 by Ye and Gao, et al. (1979) (S5).

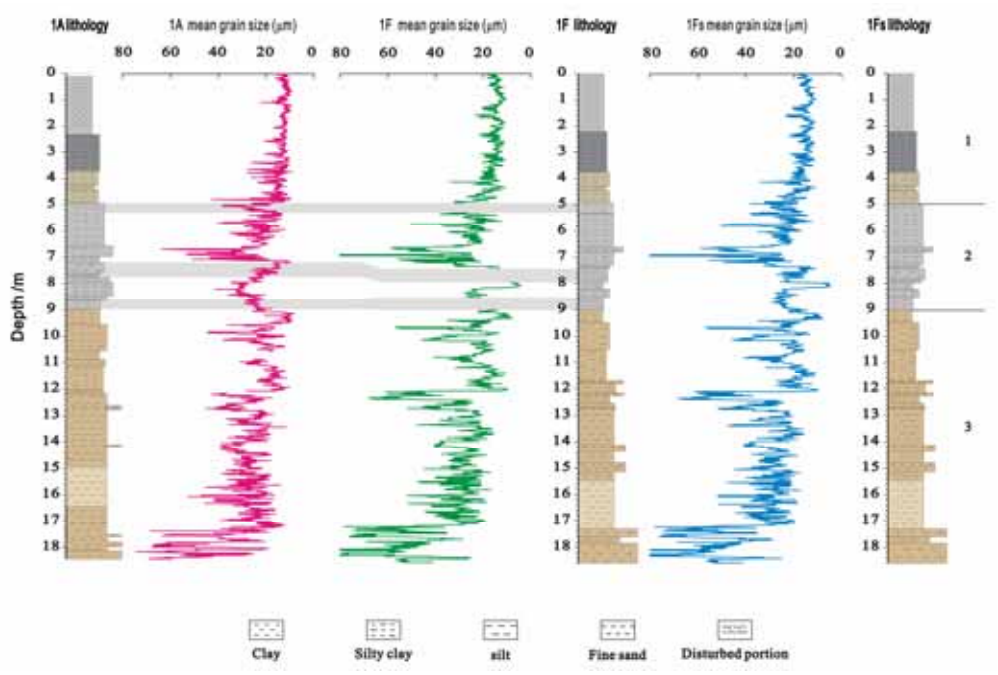

Fig. S4 Comparison of lithology and mean grain size of cores 1A and 1F and the composite core 1Fs. Following conventional methods, we calibrated core depth with the wire length, and then built calibrated depths for our cores. Because parts of core 1F were disturbed or mixed by drilling mud, we discarded these portions. According to comparisons of lithology and curves of mean grain size between cores 1F and 1A, we replaced the disturbed portions of 1F (4.93-5.29, 7.42-7.96 and 8.54-8.98 m) by the equivalent portions of the parallel core 1A (4.94-5.28, 7.19-7.76 and 8.61-8.98 m), and constructed a composite column (1Fs). Horizontal gray bars between cores mark the zones of disturbed sediments in core 1F and corresponding portions of core 1A. Gray lines and numbers to the right of 1Fs indicate generalized lithologic units. 1: 0–4.99 m, dark gray to light brown lacustrine silty clay or clay with horizontal beddings; 2: 4.99–9.01 m, gray and gray-yellowish silty clay with silt layers; 3: 9.01–18.61 m, light brown and gray silty clay, loess-like silt and fine sand layers in the lower part.

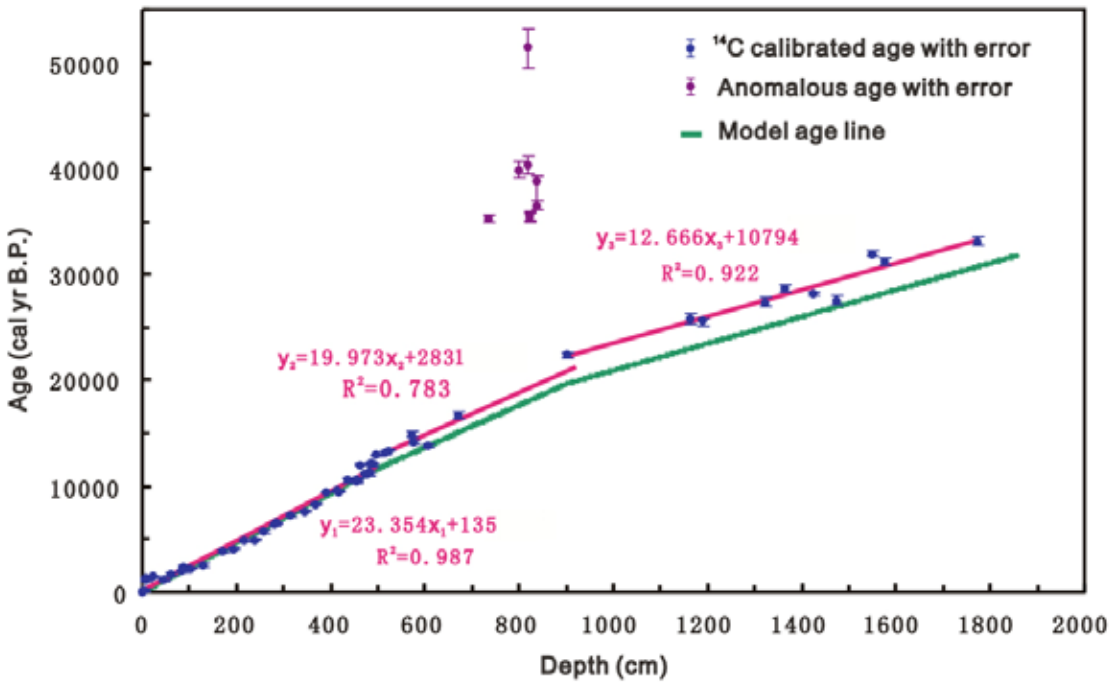

Fig S5. The relationship between calibrated ^{14}C age and depth. The anomalous data points in purple were not used in establishing the chronology (see Materials and Methods for interpretation and model description).

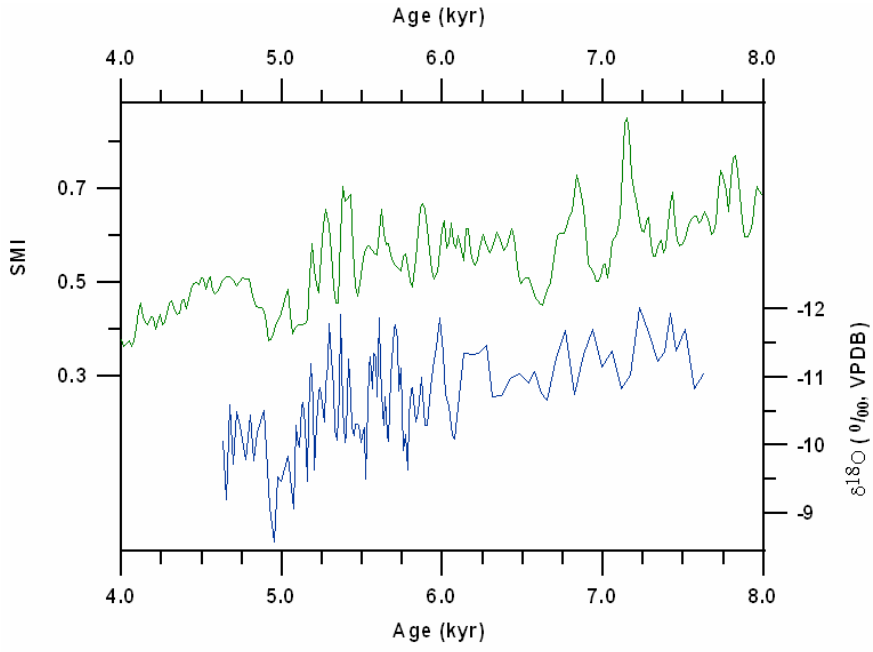

Fig. S6 Comparison of SMI for core 1Fs (green, summer monsoon index, a nondimensional index derived from normalized and averaged $CaCO_3$ and TOC flux--see detail in the text) and $\delta^{18}O$ of the Xiannv Cave (blue, S6). The Xiannv Cave speleothem record has an independent timescale provided by ICP-MS ^{230}Th ages from isotope laboratory of University of Minnesota. When we adjusted the SMI profile 150 yrs younger than our model time scale, these two records show a remarkable resemblance during the period of 4.6-7.6 ka (the correlation coefficient increased from 0.42 to 0.47 after adjustment), indicating that the reservoir effect on ^{14}C ages in our record for this time interval is likely a little older than the mean reservoir age (135 yrs) for the Holocene (Fig. 2). This comparison implies that fluctuations in the reservoir effect may exist on shorter time scales, while 135 yrs represent an average estimate of the reservoir effect for the whole Holocene. This comparison also supports our chronology and suggests that the Holocene reservoir age of Lake Qinghai sediments is not more than 1000 yrs as previously suggested (S7).

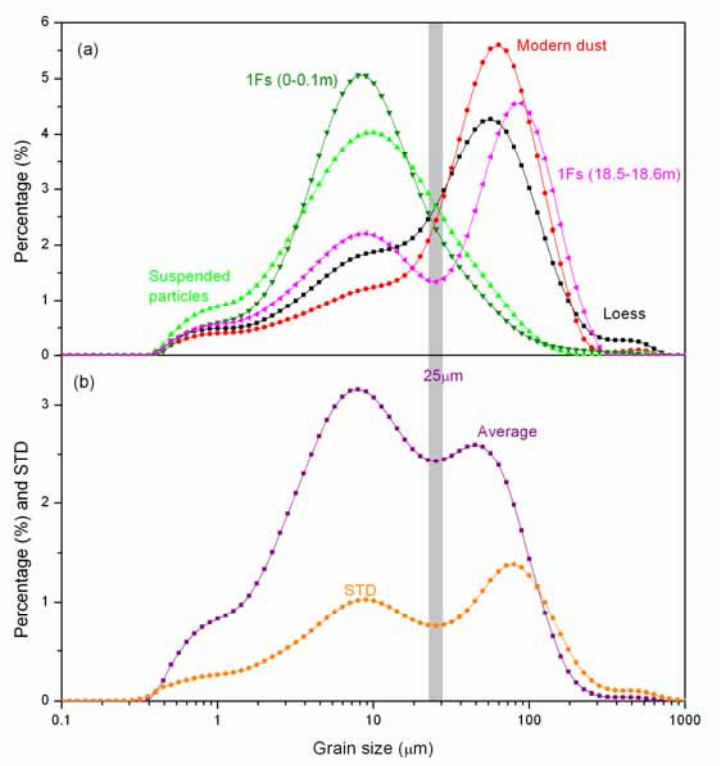

Fig. S7 a) Grain size distributions of modern dust (red), suspended particles from the Buha River (light green), eolian loess (black) from the area surrounding Lake Qinghai, top 10 cm lacustrine sediments (dark green), and bottom 10 cm loess-like sediments (pink) of core 1Fs; **b**) Distribution patterns of averaged percentage (purple) and standard deviations (orange) of each grain size class for all samples from core 1Fs. Gray bar at 25 μm indicates the boundary between fine and coarse populations, taken as the threshold between the dominance of riverine and eolian contributions to lake sediments.

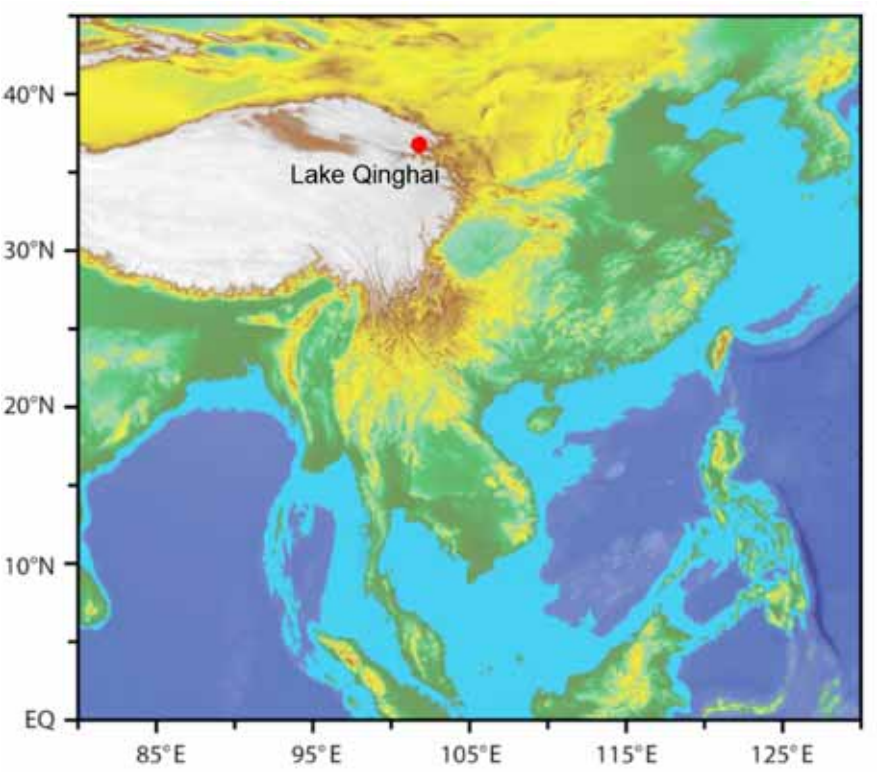

Fig. S8 Regional relief of southeastern Asia (GTOPO30 data distributed by U.S. Geological Survey's EROS Data Center). Light blue denotes areas of marginal seas emergent during the LGM when the sea level was ~130 m lower than present. It also demonstrates that the coastline in eastern China shifted eastward by ~1000 km during the LGM (S8).

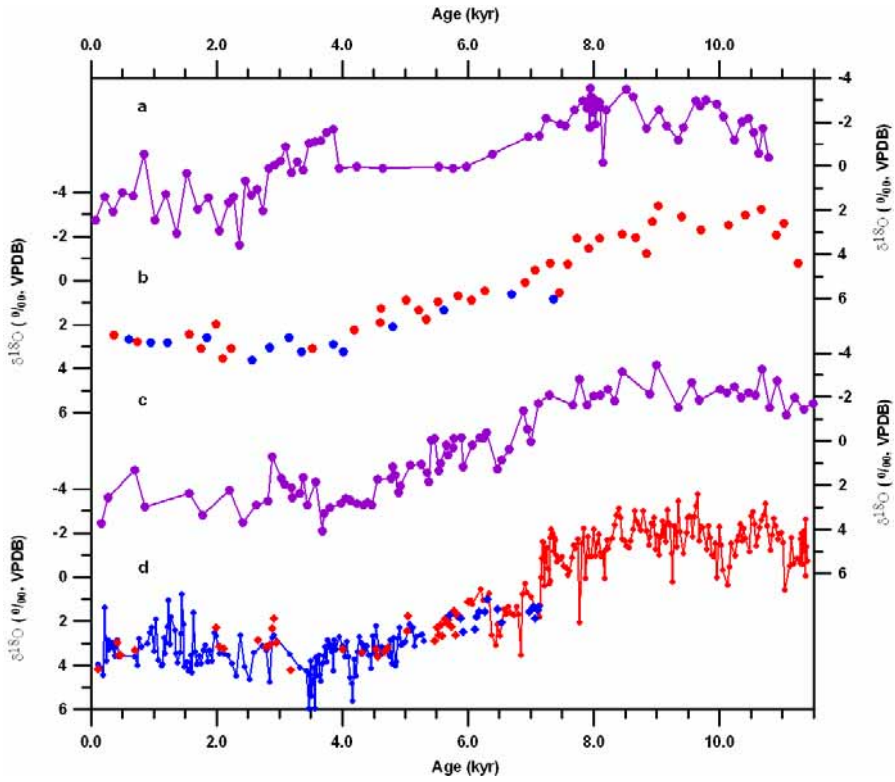

Fig. S9 Comparisons among ostracod $\delta^{18}O$ results from Lake Qinghai sediments. **a**) Zhang et al., 1994 (S9); **b**) Lister et al., 1991 (S10); **c**) Liu et al., 2007 (S11); **d**) this study. Blue indicates *L. inopinata* and red for *E. mareotica*. Purple shows ostracod $\delta^{18}O$ without species classification. We subtracted 135 yr (the Holocene reservoir effect estimated here) from calibrated ages (by CALIB 510 (S12)), which were derived from the original conventional radiocarbon ages (S13) in cores QH85-16A, QH85-14B, and QH2000, respectively, and then established the sample ages by linear interpolation for curves **a**, **b** and **c**. Our high resolution ostracod $\delta^{18}O$ curve shows a similar trend to all curves mentioned above but with more detail.

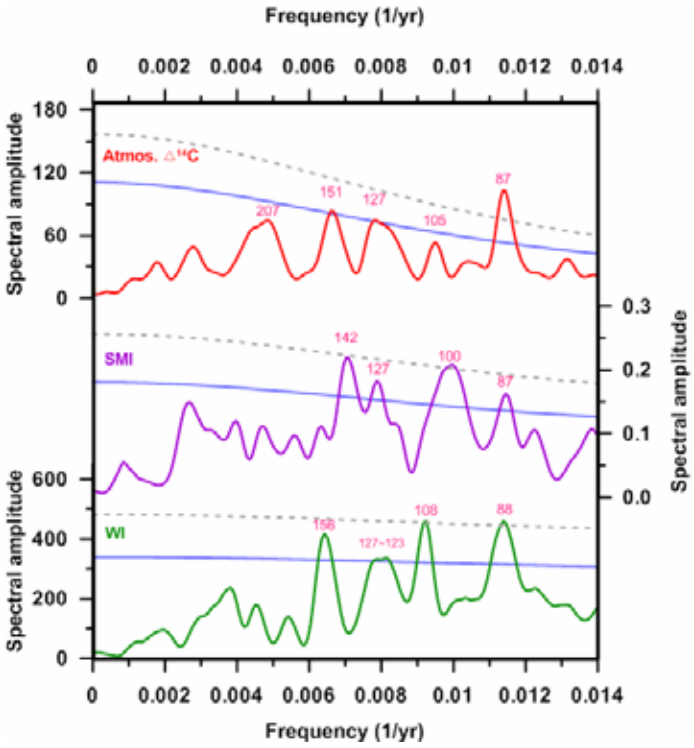

Fig. S10 Power spectra of atmospheric $\Delta^{14}C$, Asian summer monsoon index (SMI) and Westerlies climate index (WI, flux of > 25 μm fraction) for core 1Fs during the last 11.5 ka. Blue and grey dashed lines are 90% and 99% significance levels, respectively. The spectra were obtained using REDFIT software (S14). The number of Welch-overlapped-segment-averaging is 6, OFAC is 4 and HIFAC is 1. All data were detrended using a first-difference filter to emphasize the high frequency component of the spectra.

Supplementary Text

Text S1: The indications of a minor role of the winter monsoon on the Lake Qinghai area

Diagnoses of modern climatological data for the Lake Qinghai area, based on the NCEP/NCAR reanalysis (S3), show that the Westerlies are predominant in the 10 m wind field in January (Fig. S3-a1) over Lake Qinghai and the Asian summer monsoon prevails in July (Fig. S3-a2). These observations are consistent with the results from ECWMF data (S15, Figs not shown). Comparison between the 10 m wind fields in January and July shows that the boundary between the winter monsoon and the summer monsoon mainly occurs over the low-elevation regions of central and eastern China. This situation contrasts with that at Lake Qinghai (3194m), which is under the influence of westerly winds rather than the winter monsoon in January, and under the influence of the summer monsoon in July. The 600 hPa wind flow fields (approx. 800m above Lake Qinghai) also demonstrate that west is the dominant wind direction in January (Fig. S3-a3) and that the Asian summer monsoon prevails in July (Fig. S3-a4). Furthermore, modeling results from PMIP2 indicate that the 10 m wind fields (Fig. S3-b1 and b2) and the 600 hPa wind flow fields (Fig. S3-b3 and b4) during the LGM are basically similar to those of modern time.

Previous studies have demonstrated that 700 hPa (approx. 3000 m) is a threshold altitude for contrasts in temperature and pressure between the east and west sides of the Tibetan Plateau. Below this threshold altitude, the winter monsoon (associated with the shallow Siberian High) has a large impact on winter wind fields, whereas above this altitude, the Westerlies are the predominant wind system (S4, S5, S16).

Newton (Fig. S3-c1, S4, S16) first showed that the wind torque due to the huge mass of the Tibetan Plateau changes sign at an altitude of about 3 km in winter, implying that below this altitude, the pressure of the eastern side of the plateau is higher than that of the western side due to the prevalence of the high-pressure winter monsoon.

Shon and Li (Fig. S3-c2, S5) calculated the temperature difference between the eastern and the western sides of the plateau. They found that below an altitude of

approximately 3 km, temperature of the eastern side ($T_{120°E}$) is colder than that of the western side ($T_{60°E}$) due to the intrusion of the cold-temperature northerly winter monsoon. These contrasts may be attributed to the fact that the Siberian High (Asian winter monsoon) is a shallow system, and they also imply that wind torque over the mountain results from thermal, as well as the mechanical, effects.

These data demonstrate that during both modern times and the LGM, the Westerlies are the predominant wind direction over Lake Qinghai in winter, while the shallow winter monsoon system only prevails over the low-elevation regions of central and eastern China. In contrast, the Asian summer monsoon can reach and influence the region of Lake Qinghai in summer.

Supplementary Tables

Table S1: Age data obtained from the cores 1F and 1A of Lake Qinghai

Lab Code	Depth (cm)	Date material	^{14}C age		Calibrated age (cal yr BP)		
			(yr BP)	Error (yr)	Lower	Upper	Median
AA78739	1	TOC	30	30	30	140	60
AA78740	5	TOC	200	35	80	310	180
XA2718	8	TOC	1210	40	1060	1260	1140
XA1748	9	TOC	1430	30	1290	1380	1330
XA2730	21	TOC	1550	20	1390	1520	1470
XA2771	44	TOC	1220	40	1060	1270	1150
XA2770	62	TOC	1780	40	1570	1820	1700
XA2769	83	TOC	2000	40	1870	2060	1950
XA2721	86	TOC	2310	30	2190	2360	2340
XA2711	104	TOC	2180	20	2130	2310	2240
XA2768	128	TOC	2470	40	2360	2710	2560
XA2766	171	TOC	3565	40	3720	3970	3865
XA2713	194	TOC	3740	20	3990	4220	4110
XA2765	215	TOC	4340	40	4840	5040	4920
XA2764	238	TOC	4380	40	4860	5050	4940
XA2763	257	TOC	4990	50	5610	5890	5720
XA2700	282	TOC	5570	20	6310	6400	6350
AA77753	284*	TOC	5680	40	6350	6600	6465
XA1755	284*	TOC	5735	40	6410	6640	6530
XA2762	316	TOC	6270	40	7030	7270	7210
XA2759	344	TOC	6780	55	7520	7720	7630
XA2758	368	TOC	7510	40	8200	8400	8335
XA2716	391	TOC	8450	30	9440	9530	9485
XA2757	412	TOC	8600	50	9500	9680	9560
XA1756	413*	TOC	8600	40	9500	9670	9550
AA77758	413*	TOC	8560	50	9470	9660	9530
AA77711	416	seed	8540	50	9470	9580	9520
XA2756	434	TOC	9430	50	10520	11060	10660
AA77712	454	seed	9280	50	10280	10580	10460
XA2755	455	TOC	9370	50	10430	10720	10590
AA77760	456	TOC	9410	60	10430	11060	10640
XA3200	463	TOC	10235	30	11830	12080	11990
XA1586	475*	seed	9670	40	10790	11200	11110

XA1751	475*	seed	9790	40	11170	11250	11215
AA77708	475*	seed	9700	60	10790	11240	11120
AA78019	477	TOC	9755	60	10880	11270	11190
XA2701	480	TOC	9900	45	11210	11590	11290
AA77761	481	TOC	9890	50	11200	11600	11290
XA3195	485	TOC	10290	30	11840	12230	12070
XA3194	490	TOC	10310	30	11990	12350	12100
XA1752	497	seed	11020	35	12880	13050	12940
XA2754	514	TOC	11280	60	13080	13270	13170
XA3210	521	TOC	11510	30	13270	13430	13350
XA3226	572	TOC	12630	40	14670	15130	14910
XA2752	577	TOC	12230	50	13920	14250	14090
AA77765	605	TOC	12010	60	13750	14000	13870
XA3187	670	plant residue	14000	40	16310	17040	16680
XA3186	736	plant residue	31350	110	34920	35620	35260
XA2748	799	TOC	34470	200	38980	40540	39810
XA3228	817	plant residue	35170	205	39320	41010	40250
XA2747	818	TOC	47905	450	49990	53610	51530
XA3185	823	plant residue	31490	110	35000	35780	35370
XA3240	823	plant residue	31690	105	35230	36020	35550
XA3184	838	plant residue	33620	140	38190	40460	38730
XA3966	838	plant residue	32230	130	35980	36860	36440
AA78823	901	TOC	18820	130	22130	22590	22360
XA3229	1162	TOC	21680	70	25370	26420	25880
XA3963	1189	TOC	21190	70	25390	26000	25570
XA2777	1323	TOC	22620	100	26960	27730	27370
XA2705	1363	TOC	23900	90	28380	29150	28730
XA2776	1425	TOC	23350	160	27910	28330	28130
XA2775	1473	TOC	22810	100	27070	27880	27540
AA77785	1550	TOC	27250	335	31690	32200	31940
XA2774	1574	TOC	26330	150	30810	31510	31210
AA77790	1773	TOC	28670	300	32665	33605	33150

*Average age of the same depth is used in establishing the age model.

Samples with shadow were collected from core 1A

Table S2: Comparison of dating results for core 1F and 1A in Lake Qinghai between Xi'an (XA) and Tucson NSF (AA) AMS facilities

Lab Code	Date material	Depth (cm)	^{14}C age	
			(yr BP)	Error (yr)
XA2700*	TOC	282	5570	20
XA1755**	TOC	284	5735	40
AA77753***	TOC	284	5680	40
XA2757*	TOC	412	8600	50
XA1756**	TOC	413	8600	40
AA77758***	TOC	413	8560	50
XA1586*	seed	475	9670	40
XA1751**	seed	475	9790	40
AA77708***	seed	475	9700	60

* Samples were pretreated and measured at Xi'an AMS Center

** Samples were pretreated at NSF -AMS in Tucson and measured in Xi'an

*** Samples were pretreated and measured at NSF-AMS in Tucson

Samples with shadow were collected from core 1A

Table S3: Comparison of ^{14}C age for TOC and seeds at the similar depths from the upper 5.0 m of core 1F and 1A

Lab Code	Date material	Depth (cm)	^{14}C age	
			(yr BP)	Error (yr)
AA77758**	TOC	413	8560	60
AA77711**	seed	416	8540	50
AA77712**	seed	454	9280	50
XA2755*	TOC	455	9370	50
XA1751*	seed	475	9790	40
AA78019**	TOC	477	9755	60

* Lab code of Xi'an AMS Center, China

** Lab code of NSF-AMS lab in Tucson

Samples with shadow were collected from core 1A

Table S4: ^{14}C dating results for surface sediment at the 1F core site, for living naked carp and algae.

Lab code	Depth(cm)	Dating material	^{14}C age (yr BP)
AA78739	0-1	TOC	30±30
AA78728		algae	post-bomb
AA78729		algae	post-bomb
AA78730		Living naked carp (*Gymnocypris przewalskii*)	post-bomb

References for Supplementary Materials:

S1. An, Z. S. *et al*. Changes of the monsoon-arid environment in China and growth of the Tibetan Plateau since the Miocene. *Quatern. Sci.* **26**, 678-693 (2006) (in Chinese with English abstract).

S2. Braconnot, P, *et al*. Results of PMIP2 coupled simulations of the Mid-Holocene and Last Glacial Maximum; Part 1: experiments and large-scale features. *Clim. Past* **3**, 261-277 (2007).

S3. Kalnay, et al. The NCEP/NCAR 40-year reanalysis project. *Bull. Am. Meteor. Soc.* **77**, 437-470 (1996).

S4. Newton, C. W. Mountain torques in the global angular momentum balance. *J. Atmos. Sci.* **28**, 623–628 (1971).

S5. Ye, D. Z. & Gao, Y. X. The Meteorology of Qinghai Tibetan Plateau (Science Press, Beijing) (in Chinese) (1979).

S6. Cai, Y. J., An, Z. S., Cheng, H., Edwards, R. L. & Tan, L. Climate changes in northeastern margin of Tibetan Plateau since 8ka BP --- The speleothem records AGU Fall meeting, San Francisco, CA. (2008).

S7. Shen, J., Liu, X. Q., Wang, S. M. & Matsumoto, R. Palaeoclimatic changes in the Qinghai Lake area during the last 18,000 years. *Quatern. Int.* **136**, 131-140 (2005).

S8. An, Z. S. et al. Paleomonsoons of China over the past 130,000 years—Paleomonsoons variation. *Sci. in China Ser. B* **34**, 1016-1024 (1991).

S9. Zhang, P. X., Zhang, B. Z., Qian, G. M., Li, H. J. & Xu, L. M. The study of paleoclimatic parameter of Qinghai Lake since Holocene. *Quatern. Sci.* **3**, 225-238 (1994) (in Chinese with English abstract).

S10. Lister, G. S., Kelts, K. R., Chen, K. Z., Yu, J. Q. & Niessen, F. Lake Qinhai,

China: Closed-basin lake levels and the oxygen isotope record for ostracoda since the latest Pleistocene. *Palaeogeogr. Palaeoclimatol. Palaeoecol.* **84**, 141-162 (1991).

S11. Liu, X. Q., Shen, J., Wang, S. M., Wang, Y. B. & Liu, W. G. Southwest monsoon changes indicated by oxygen isotope of ostracode shells from sediments in Qinghai Lake since the late Glacial. *Chin. Sci. Bull.* **52**, 539-544 (2007).

S12. Reimer, P. J. *et al.* IntCal04 terrestrial radiocarbon age calibration, 0–26 Cal kyr BP. *Radiocarbon* **46**, 1029-1058 (2004).

S13. Colman, S. M., Yu, S. Y., An, Z. S., Shen, J. & Henderson, A. C. G. Late Cenozoic climate changes in China's western interior: a review of research on Lake Qinghai and comparison with other records. *Quatern. Sci. Rev.* **26**, 2281-2300 (2007).

S14. Schulz, M. & Mudelsee M. REDFIT: estimating red-noise spectra directly from unevenly spaced paleoclimatic time series. *Comput. Geosci.* **28**, 421- 426 (2002).

S15. ECMWF ERA-40 data used in this study/project have been provided by ECMWF/have been obtained from the ECMWF Data Server.

S16. Newton, C. W. Global angular momentum balance: earth torques and atmospheric fluxes. *J. Atmos. Sci.* **28**, 1329–1341(1971).